VBPRM reduced the distance that the camera traveled, while it was unable to see, by 71%–94%. Thus, the occlusion-aware planner made significant reductions to the distance that the camera must travel while it was unable to see the target. Simulations of different tasks showed similar reductions in penalized distance.

V. CONCLUSION

This paper introduced the VBPRM planner to compute paths that involve constraints that are inherent to industrial manipulators with the constraints of placing and orienting a camera in space. This research aims to provide manipulators, such as those found on assembly lines, with the capability to perform vision-based tasks that require motions with linear interpolation of joint positions, collision avoidance, and observation an image target with an onboard camera. Our strategy is based on extending the PRM by weighting the edges of the graph according to the visibility of a fixed target. Results presented in this paper demonstrate the value of the VBPRM for tasks that require a robot equipped with an eye-in-hand camera to move while avoiding collisions with obstacles and keeping a target within its sight.

Future work will include performance improvements, particularly in the visibility penalty computation, which would benefit greatly from acceleration structures, such as an adaptively sampled distance field [16] for the geometric tests. Our experiments were conducted using a uniformly sampled road map; however, a road map whose vertices were sampled using a visibility or collision property as a bias function could potentially see improved results.

The VBPRM provides a practical path planner to compute motions that satisfy vision constraints of an arm-mounted camera in a cluttered environment. Its compatibility with point-to-point interfaces, which is commonly found on industrial robots, makes it suitable to provide visibility awareness to existing industrial systems.

REFERENCES

[1] L. E. Kavraki, P. Svestka, J.-C. Latombe, and M. H. Overmars, "Probabilistic roadmaps for path planning in high-dimensional configuration space," *IEEE Trans. Robot. Autom.*, vol. 12, no. 4, pp. 566–580, Aug. 1996.

[2] F. Chaumette and S. Hutchinson, "Visual servo control Part I: Basic approaches," *IEEE Robot. Autom. Mag.*, vol. 13, no. 4, pp. 82–90, Dec. 2006.

[3] G. Chesi, K. Hashimoto, D. Prattichizzo, and A. Vicino, "Keeping features in the field of view in eye-in-hand visual servoing: A switching approach," *IEEE Trans. Robot.*, vol. 20, no. 5, pp. 908–913, Oct. 2004.

[4] K. Hashimoto and T. Noritsugu, "Potential switching control in visual servo," in *Proc. IEEE Int. Conf. Robot. Autom.*, Apr. 2000, pp. 2765–2770.

[5] N. Mansard and F. Chaumette, "A new redundancy formalism for avoidance in visual servoing," in *Proc. IEEE/RSJ Int. Conf. Intell. Robots Syst.*, Edmonton, AB, Canada, Aug. 2005, pp. 468–474.

[6] P. I. Corke and S. A. Hutchinson, "A new partitioned approach to image-based visual servo control," *IEEE Trans. Robot. Autom.*, vol. 17, no. 4, pp. 507–515, Aug. 2001.

[7] E. Malis, F. Chaumette, and S. Boudet, "2-1/2-d visual servoing," *IEEE Trans. Robot. Autom.*, vol. 15, no. 2, pp. 238–250, Apr. 1999.

[8] Y. Mezouar and F. Chaumette, "Path planning for robust image-based control," *IEEE Trans. Robot. Autom.*, vol. 18, no. 4, pp. 534–549, Aug. 2002.

[9] F. Schramm, F. Geffard, G. Morel, and A. Micaelli, "Calibration free image point path planning simultaneously ensuring visibility and controlling camera path," in *Proc. IEEE Int. Conf. Robot. Autom.*, Roma, Italy, Apr. 2007, pp. 2074–2079.

[10] B. Thuilot, P. Martinet, L. Cordesses, and J. Gallice, "Position based visual servoing: Keeping the object in the field of vision," in *Proc. IEEE Int. Conf. Robot. Autom.*, Washington, DC, May 2002, pp. 1624–1629.

[11] K. Tarabanis, R. Y. Tsai, and A. Kaul, "Computing occlusion-free viewpoints," *IEEE Trans. Pattern Anal. Mach. Intell.*, vol. 18, no. 3, pp. 279–292, Mar. 1996.

[12] T. H. Cormen, C. E. Leiserson, R. L. Rivest, and C. Stein, *Introduction to Algorithms*, 1st ed. Cambridge, MA: MIT Press, 1997.

[13] F. Schwarzer, M. Saha, and J.-C. Latombe, "Adaptive dynamic collision checking for single and multiple articulated robots in complex environments," *IEEE Trans. Robot.*, vol. 21, no. 3, pp. 338–353, Jun. 2005.

[14] S. Leonard, E. A. Croft, and J. J. Little, "Dynamic visibility checking for vision-based motion planning," in *Proc. IEEE Int. Conf. Robot. Autom.*, Los Angeles, CA, May 2008, pp. 2283–2288.

[15] E. Trucco and A. Verri, *Introductory Techniques for 3-D Computer Vision*. Englewood Cliffs, NJ: Prentice-Hall, 1998.

[16] S. Frisken, R. Perry, A. Rockwood, and T. Jones, "Adaptively sampled distance fields: A general representation of shape for computer graphics," in *Proc. 27th Annu. Conf. Comput. Graph. Interactive Techn.*, 2000, pp. 249–254.

Autonomous Robotic Pick-and-Place of Microobjects

Yong Zhang, *Student Member, IEEE*,
Brandon K. Chen, *Student Member, IEEE*,
Xinyu Liu, *Student Member, IEEE*,
and Yu Sun, *Senior Member, IEEE*

Abstract—This paper presents a robotic system that is capable of both picking up and releasing microobjects with high accuracy, reliability, and speed. Due to force-scaling laws, large adhesion forces at the microscale make rapid, accurate release of microobjects a long-standing challenge in micromanipulation, thus representing a hurdle toward automated robotic pick-and-place of micrometer-sized objects. The system employs a novel microelectromechanical systems (MEMS) microgripper with a controllable plunging structure to impact a microobject that gains sufficient momentum to overcome adhesion forces. The performance was experimentally quantified through the manipulation of 7.5–10.9 μm borosilicate glass spheres in an ambient environment. Experimental results demonstrate that the system, for the first time, achieves a 100% success rate in release (which is based on 700 trials) and a release accuracy of 0.45$\pm$0.24 μm. High-speed, automated microrobotic pick-and-place was realized by visually recognizing the microgripper and microspheres, by visually detecting the contact of the microgripper with the substrate, and by vision-based control. Example patterns were constructed through automated microrobotic pick-and-place of microspheres, achieving a speed of 6 s/sphere, which is an order of magnitude faster than the highest speed that has been reported in the literature.

Index Terms—Adhesion forces, automated operation, microelectromechanical systems (MEMS) microgrippers, micromanipulation, robotic pick-and-place.

I. INTRODUCTION

The past decade has witnessed significant efforts in the pursuit of automated robotic operation at the micrometer scale [1]. Among many types of microrobotic operation, pick-and-place of microobjects promises specificity, precision, and programmed motion, which are

the features that make microrobotic manipulation amenable to automation for the construction of microsystems. Targeting automated robotic microassembly, many techniques and systems have been developed [1]–[11]. Notably, snap–lock interfaces were employed in some of these systems [6], [8], [11] to circumvent the difficulty of releasing microobjects due to strong adhesion forces at the microscale (e.g., van der Waals, electrostatic, and capillary forces) [12].

This paper deals with the scenario where microobjects are free of mating interfaces [13]–[15]. Microrobotic pick-and-place of free microspheres has been used to build diamond-shaped structures by assembling microspheres into a lattice for photonic use [13]. Based on a combination of microfabrication and micromanipulation [14], novel photonic crystals were demonstrated.

State-of-the-art pick-and-place of microobjects is skill-dependent and entails repeated trial-and-error efforts. One important difficulty is that strong adhesion forces make the microobject adhere to the end-effector during release. To ease the difficulty of release, several approaches have been proposed in the past decade, which can be classified into two categories: passive-release techniques and active-release techniques.

Passive-release techniques rely on the contact between the microobject and the substrate to detach the microobject from the end-effector. In consideration of adhesional and rolling-resistance factors [16], microspheres were rolled on an Au-coated substrate for both pick and release, thereby causing the fracture of the sphere–substrate interface and the sphere–tool interface, respectively. Similarly, it was also demonstrated that substrates with an ultraviolet-cure adhesive [17] or a gel film [10] were used to facilitate release. Another passive-release technique uses the edge of the substrate to scrape the adhered object off the tool [18]. A commonality of passive-release techniques is the dependence on surface properties of substrates, it is time-consuming, and it has poor repeatability.

By contrast, active-release methods intend to detach the microobject from the end-effector without touching the substrate. By applying a voltage between the probe and the substrate [19], an electric field was created to detach the object from the probe. However, this method requires the microobject, the probe, and the substrate all to be conductive. More importantly, the released microobjects landed at random locations on the substrate, which resulted in a poor release accuracy.

The second type of active release makes use of mechanical vibration [20]. Requiring a large bandwidth of the manipulator, the vibration-based method takes advantage of inertial effects of both the end-effector and the microobject to overcome adhesion forces. The release process has been modeled and simulated to predict the landing radius of the released object [21]; however, the accuracy has not been experimentally quantified. The third type of active release employs vacuum-based tools [22] to create a pressure difference for both pick and release. However, miniaturization and accurate control of vacuum-based tools can be difficult, and its use in a vacuum environment can be limited. Finally, micro-Peltier coolers were used to form ice droplets instantaneously for pick-and-place of microobjects [23]. Thawing of the ice droplets was used to release objects. The freezing–heating approach is restricted to micromanipulation in an aqueous environment.

Besides probe-based techniques, micromanipulation with microelectromechanical systems (MEMS) microgrippers [24]–[29] has also been widely reported. Although these double-ended microgrippers significantly facilitate the pick-up step, they further exacerbate the release issue since the microobject always adheres to one of the gripping arms. Well-known methods for the reduction of adhesion forces between the microobject and the gripping arms are the creation of rugged gripping arms [24] and chemically coated gripping arms [28]. However, the effectiveness of gripping-arm treatment for release is limited, since the
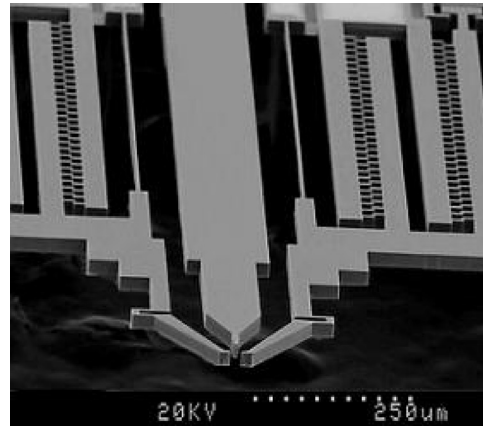
Fig. 1. SEM image of a three-pronged microgripper capable of both grasping and active release of microobjects.

decreased amount of adhesion forces is often still strong enough to keep the microobject adhering to one of the gripping arms.

In this paper, we present an active-release strategy using an MEMS microgripper that is integrated with a plunging structure between two gripping arms, as shown in Fig. 1. While this method retains the advantage of double-ended tools to pick up microobjects, the plunger is capable of thrusting a microobject adhering to a gripping arm to a desired destination on a substrate, thus enabling highly repeatable release with an accuracy of 0.45 ± 0.24 μm. The results were obtained under an optical microscope with 7.5–10.9 μm borosilicate microspheres on glass substrates in an ambient environment. No surface treatments were conducted to the microgripper, microspheres, or substrates.

Enabled by the grasping and release capabilities, the microrobotic system achieved fully automated pick-and-place of microspheres at a speed of 6 s/sphere. This speed is an order of magnitude higher than the highest speed reported in the literature [13]. Image processing is used to recognize features, such as the gripping arms and microspheres. The system detects the contact between the microgripper and the substrate purely through visual feedback without using additional force/touch sensors. Automated pick-and-place was performed through vision-based control.

Device details and preliminary results of release accuracy quantification were reported in [30]. New results described in this paper include refined experimental results to quantify release accuracy and new experimental results of automated robotic pick-and-place of microspheres.

II. THREE-PRONGED MICROGRIPPER

Fig. 2 shows a schematic of the microgripper. The monolithic device integrates three electrostatic microactuators to drive two normally open gripping arms as well as a plunger for active release. In this design, electrostatic actuation was chosen over electrothermal actuation because the temperature rise of the gripping arms can influence adhesion forces and reduce the consistency of device performance. Furthermore, electrostatic actuation was also chosen to drive the plunger because it exhibits a much higher bandwidth than electrothermal actuators and is able to deliver a much faster speed, thus representing an important advantage to thrust off an adhered microobject.

This design is different from existing microgrippers that have either only one actively actuated gripping arm [27], [28] or two interdependently active gripping arms [26]. Since to which gripping arm a microobject adheres is random, both gripping arms in our design have an independent actuator to position the adhered object in order to properly
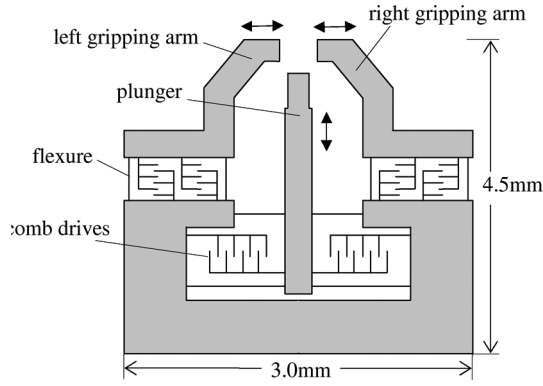
Fig. 2.   Microgripper schematic.
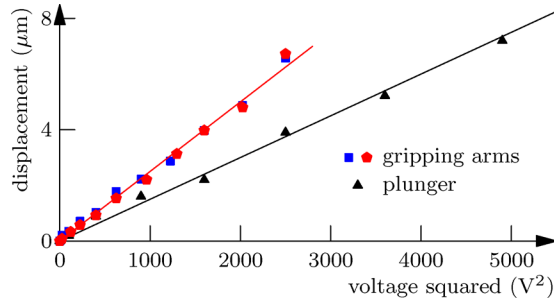
Fig. 3.   Characterized microactuator performance.
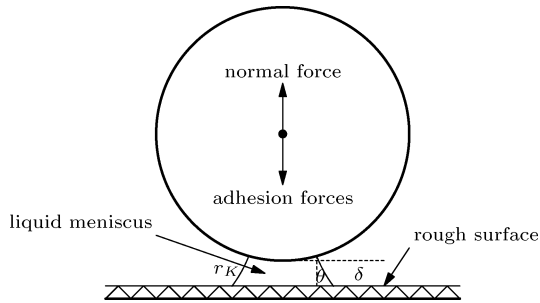
Fig. 4.   Adhesion forces acting on a microsphere on a rough surface.

align to the plunger for release. The devices were microfabricated using a modified deep reactive-ion etching (DRIE) on silicon-on-insulator (SOI) process [28] with a 25-μm-thick device silicon layer. Fig. 3 shows the characterized actuation performance.

III. FORCE ANALYSIS OF THE PICK-AND-PLACE PROCESS

Adhesion forces in an ambient environment include three types of attractive forces, namely, the van der Waals force, the electrostatic force, and the capillary force, all of which depend on the separation distance δ, between a microsphere and a flat surface it adheres to. Fig. 4 shows a microsphere adhered to a flat surface with surface roughness exaggerated.

The van der Waals force [31] is given by

$$F_{\mathrm{vdw}} = \left(\frac{\delta}{\delta + r/2} \right)^2 \left(\frac{Hd}{16\pi\delta^2} + \frac{H\rho^2}{8\pi\delta^3} \right) \tag{1}$$

where r is the roughness of the flat surface, H is the Lifshitz–van der Waals constant that ranges from 0.6 eV for polymers to 9.0 eV

for metals, d is the microsphere diameter, and ρ is the radius of the adhesion surface area.

To estimate the van der Waals force between a 10-μm borosilicate microsphere and the sidewall of a gripping arm, δ is assumed to be 0.35 nm [32], ρ is assumed to be 0.65% of the radius of the microsphere [32], H is assumed to be 7.5 eV [32], and r is assumed to be 100 nm. Thus, the van der Waals force is calculated to be 1.51×10^{-4} μN.

The electrostatic force [33] is given by

$$F_{\mathrm{elec}} = \frac{\pi \epsilon d U^2}{2\delta} \tag{2}$$

where ϵ is the permittivity of air, and U is the voltage difference between the microsphere and the flat surface. When U is assumed to be 0.40 V [32], the electrostatic force between a 10-μm microsphere and the sidewall of a gripping arm is calculated to be $6.36 \times 10^{-2}\mu$N.

The third type of attractive force is the capillary force [34], which is given by

$$F_{\mathrm{cap}} = \frac{2\pi d\gamma \cos\theta}{1 + \delta/(2r_K \cos\theta - \delta)} \tag{3}$$

where γ is the liquid surface tension, which is 0.073 N·m^{-1} for water at 22 °C, θ is the contact angle of the meniscus with the microsphere, and r_K is the Kelvin radius, which is defined as the mean radius of the curvature of the liquid–vapor interface.

To estimate the capillary force exerted on a 10-μm microsphere by a water meniscus at room temperature, θ is assumed to be 10°, δ is still assumed to be 0.35 nm, as for the calculation of the van der Waals force, and r_K is assumed to be 1 nm. The capillary force is calculated to be 3.71 μN.

It can be seen that the van der Waals force is the smallest among the three attractive forces and heavily depends on the roughness of the surface. Since devices were formed through DRIE, which produces scallop structures on the sidewalls of the gripping arms, the rough surface makes the van der Waals force negligible. The electrostatic force depends on the voltage difference, which is difficult to accurately estimate when the microsphere is nonconductive. Unlike the van der Waals force and electrostatic force, neither of which requires physical contact, the capillary force in the air results from a phenomenon, which is called capillary condensation [33]. Liquid from the vapor phase condenses between sufficiently close asperities and forms menisci that cause the capillary force. Thus, there exists a working range, beyond which, the capillary force as well as the liquid menisci disappear.

Fig. 5 illustrates forces exerted on a microsphere by the gripping arms and/or the substrate during grasping and release. Fig. 5(a)–(c) shows the side view, and Fig. 5(d)–(f) shows the top view. Fig. 5(a) shows that the microgripper approaches the microsphere and uses the gripping arm to laterally push it in order to break the adhesion bond between the microsphere and the substrate. F_s is the adhesion forces, N_s is the normal force from the substrate, N_r is the lateral pushing force applied by the right gripping arm, and F_r is the adhesion forces from the gripping arm in the normal direction. Upon the application of N_r, the stress distribution in the contact area between the microsphere and the substrate becomes nonuniform, which creates a rolling-resistance moment M_s [35]. Besides the adhesion forces F_s and F_r that are normal to the flat surfaces, f_s and f_r are additional capillary forces from the substrate and the gripping arm, respectively. Capillary force f_s (f_r) resists the relative motion between the microsphere and the substrate (gripping arm) through the menisci. In this situation, the total capillary forces from the substrate and gripping arm are not perpendicular to the flat surfaces.

After the microsphere is moved laterally from its original position, the two gripping arms close and grasp it, as shown in Fig. 5(b). The normal force and adhesion forces, N_l and F_l, are from the left gripping
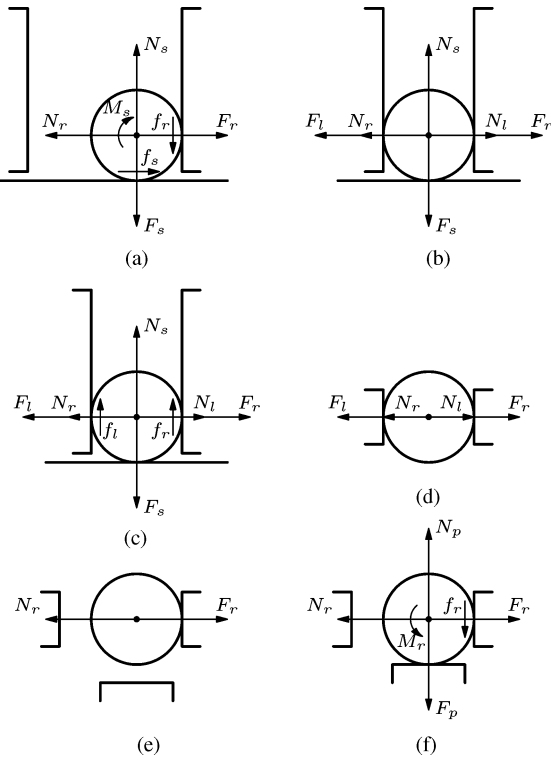
Fig. 5. Analysis of forces during grasping and active release.

Fig. 6. Experimental setup for micrograsping and active release tests. Inset shows a wire-bonded microgripper.

arm. Similarly, N_r and F_r, are from the right gripping arm. Besides F_l and F_r, there can also be additional capillary forces that are parallel to the substrate surface and gripping-arm surface, although they are not shown in the diagram for clarity.

The microgripper is then raised, as shown in Fig. 5(c), to lift up the microsphere. The additional capillary forces from the gripping arms, i.e., f_l and f_r, overcome the adhesion forces from the substrate, i.e., F_s, which decreases gradually as a function of the distance between the microsphere and the substrate.

When the microsphere is up in the air [see Fig. 5(d)], the adhesion forces from the substrate become negligible. Upon reaching a desired destination, the gripping arms are opened, during which all of the adhesion forces and normal forces from the gripping arms decrease. Consequently, the microsphere separates from one gripping arm and keeps adhering to the other gripping arm by adhesion forces, as shown in Fig. 5(e).

For release, the gripping arm with the adhered microsphere is properly positioned relative to the plunger, as shown in Fig. 5(f). The plunger is then controlled to move forward to thrust out and collide with the microsphere. Eventually, the microsphere escapes from the adhesion forces from the gripping arm by its own inertia and lands on the substrate. In Fig. 5(f), N_p is the pushing force that is applied by the plunger, F_p is the adhesion forces from the plunger, and M_r and f_r are, respectively, the rolling-resistance moment and additional capillary force from the gripping arm.

IV. EXPERIMENTAL RESULTS AND DISCUSSION

The experimental setup (see Fig. 6) consists of an optical microscope (Motic PSM-1000) with a CMOS camera (Basler A601f). A custom-made circuit board with a wire-bonded microgripper was mounted on a 3-degree-of-freedom (DOF) microrobot (Sutter MP285) at a tilting angle of 25°.
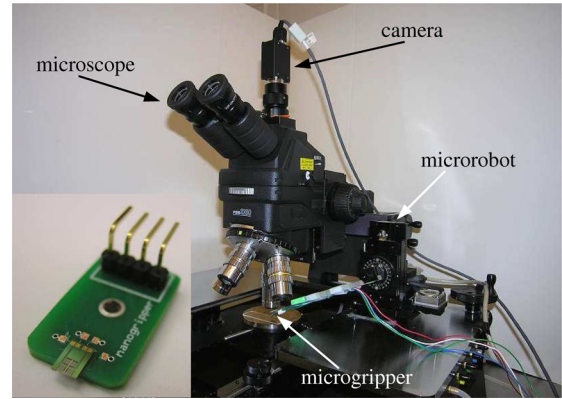
Borosilicate glass microspheres (with diameters 7.5–10.9 μm) were manipulated at a room temperature of 22 °C with a relative humidity of 50% ± 5%. A droplet of microspheres in isopropanol was micropipetted onto a microscope slide and was dried in air.

A. Repeatability of Active Release

After the gripping arms are opened, the microsphere randomly adhered to a gripping arm in all cases. For successful release, the microsphere must gain a sufficient amount of momentum from the collision with the plunger in order to overcome the adhesion forces. The speed of the plunger can be varied by controlling the rising profile of the actuation voltage. When a sharp increase in actuation voltage was applied to the plunger, release of the microsphere was guaranteed (i.e., 100% success rate, $n=700$). A high plunging speed alleviates careful sample-preparation requirements (e.g., baking) or environmental control requirements (e.g., humidity). Quantification using high-speed videography (13 000 frames/s) revealed that a plunging speed of 65.24 mm/s produced a microsphere speed of 105.01 mm/s with a momentum of 1.40×10^{-13} kg·m/s. This plunging speed guaranteed the successful release for all trials. High-speed videography also demonstrated that a microsphere was separated from the plunger upon impact.

B. Quantification of Release Performance

To quantitatively characterize release performance, single microspheres were repeatedly picked and released from different heights (2–30 μm) above the substrate. Fig. 7(a) shows representative data of landing positions on a glass substrate. The results show a fairly linear and predictable relationship between landing positions and heights from the substrate, thus indicating that forces, including the van der Waals forces and the electrostatic forces from both the substrate and the microgripper, as well as the gravitational force, do not have a significant effect on the high-speed microsphere that travels a short distance in air.

Fig. 7(a) also shows that the accuracy and precision of landing are inversely proportional to the height from the substrate. When the height was more than 20 μm, random landing locations were observed, which should be, in part, due to the more pronounced airflow effect.

As mentioned earlier, adherence of the microsphere to which gripping arm is random. Fig. 7(a) shows experimental data that are collected when the microspheres adhered to the right gripping arm. Similar data were captured but not shown for microspheres that adhered to the left gripping arm.
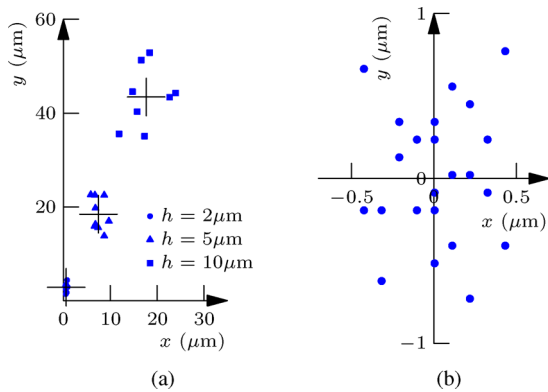
Fig. 7. Landing positions of microspheres. (a) h is the height of the gripping arms from the substrate. (b) Release height is set to 2 μm for accuracy quantification.

TABLE I
SUMMARY OF RELEASE ACCURACY

	objects adhered to left arm	objects adhered to right arm
accuracy of landing positions	$0.45 \pm 0.24 \mu$m ($n = 25$)	$0.42 \pm 0.22 \mu$m ($n = 24$)

Given the previous findings, the release height was set to 2 μm above the substrate for two purposes: to determine the average landing positions and to quantify the release accuracy. The small distance of 2 μm from the substrate reduces the distance/time that the microsphere travels in air, thus making the landing location less sensitive to environmental disturbances. The magnification of the microscope used for measurements was $100\times$ with the numerical aperture of 0.42, which, in conjunction with the camera, resulted in the pixel size of 0.11 μm $\times$ 0.11 μm.

Fig. 7(b) shows the recorded landing positions relative to the target position of the microsphere, thus proving an accuracy of 0.45 ± 0.24 μm (0.42 ± 0.22 μm) for microspheres adhering to the right gripping arm, as summarized in Table I. The 0.24-μm (0.22-μm) standard deviation of the landing positions can be due either to 1) slight variations of the initially adhering lateral and/or vertical positions of the microsphere on the gripping arm or 2) imperfect control of the release height due to the repeatability of the microrobot along the vertical direction.

In addition to a high accuracy, the active-release technique enables easy, fast pick-and-place operation. The actual release takes 0.17 ms according to high-speed videography.

C. Understanding the Curved Trajectory

Interestingly, it can be seen from Fig. 7 that the microspheres all landed to the right/left side of the plunger (plunger was along the y-axis), depending on to which gripping arm they adhered. High-speed imaging verified that the flying path of the microsphere was, indeed, curved. Images shown in Fig. 8 were taken when the gripping arms were 20 μm above the substrate.

The van der Waals force and electrostatic force decrease with increased distances between the microsphere and gripping arm. Additionally, the capillary force vanishes beyond a certain distance. Thus, it is assumed that the gripping arm has an adhesion-force effective region around it, as indicated by dashed lines in Fig. 9.

During release, the plunger first impacts the microsphere along the sidewall of the gripping arm at a high speed, as shown in Fig. 9(a), where the dashed lines represent the adhesion-force effective region. F_p and N_p are, respectively, the adhesion forces and pushing force
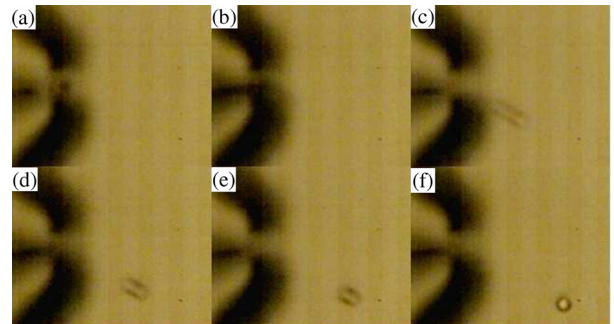
Fig. 8. High-speed videography (13 000 frames/s) quantifying microsphere trajectories upon release from a height of 20 μm above the substrate.
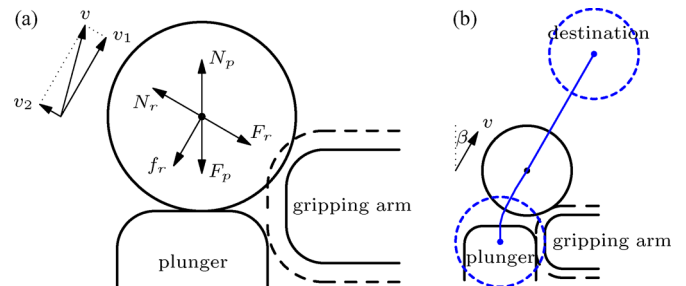
Fig. 9. Microsphere reveals a curved trajectory during active release. (a) Plunger thrusts the microsphere that reaches the roundish corner of the gripping arm. (b) Microsphere escapes from the effective range of the adhesion forces. The trajectory is drawn under the assumption that there are no disturbances when the microsphere is in the air.

from the plunger. F_r and N_r are, respectively, the adhesion forces and normal force from the gripping arm. When the traveling microsphere approaches the gripping-arm corner, which was rounded by DRIE etching, the adhesion forces create a radial acceleration toward the corner, which curves its travel direction. While the microsphere is within the adhesion-force effective region, there exists resistance f_r (additional capillary force) in the tangential direction caused by menisci. Eventually, the microsphere leaves the gripping-arm tip and, hence, the adhesion-force effective region. It then travels straightly and lands on the substrate, as depicted in Fig. 9(b). During its traveling in air, the microsphere has its gravity, as well as van der Waals forces and electrostatic forces from both the microgripper and the substrate.

V. MICROROBOTIC PICK-AND-PLACE OF MICROSPHERES

A. Recognition of Microgripper and Spheres

The microspheres on the substrate were recognized using a Hough transform to determine their centers and radii. Contours formed from Canny edge detection readily recognize the gripping arms and the plunger. As shown in Fig. 10(a), M_1, M_2, and M_3 denote the centroids of the two gripping arms and the plunger. By comparing the y-coordinates of their centroids, the left gripping arm, right gripping arm, and plunger were distinguished.

Minimum bound rectangles (MBRs) were used to further define the positions of the two gripping arms, as shown in Fig. 10(a). Point D was then taken as the overall position of the microgripper, which is the intersection of the horizontal line going through the plunger centroid M_3, and the line connecting the left adjacent corners of the top and bottom MBRs.
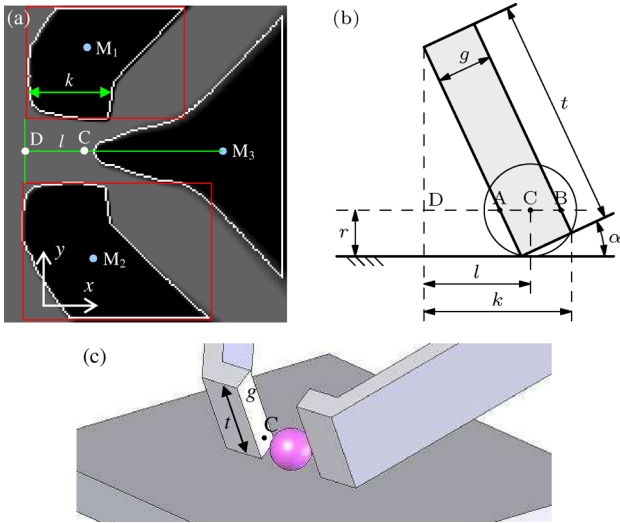
Fig. 10.   (a) Recognized gripping arms and plunger. (b) Sidewall of a gripping arm to determine the secured grasping position C. (c) Three-dimensional schematic showing the grasping of a microsphere.
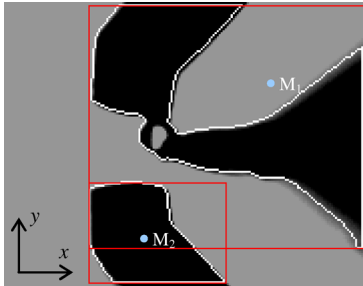
Fig. 11.   Visual determination of which gripping arm the microsphere adheres to after the gripping arms open.

To attain secured grasping, the system aligns the grasping position of the gripping arms with respect to a microsphere, as illustrated in Fig. 10(b), where g is the width of the gripping arm [which is denoted by k in Fig. 10(a)], and r is the radius of the microsphere. The contact position of the gripping arm with the microsphere is on the segment AB. In particular, the middle position C provides the most security to grasp when microspheres slide during grasping [see Fig. 10(b)]. According to the geometry, the distance from the microgripper position D to the optimal grasping position C is given by $l = t \sin \alpha + (g/2) \cos \alpha - r \cot \alpha$, which is a function of the size of the microsphere to be grasped.

When the gripping arms open, the microsphere randomly adheres to one of the two gripping arms. As shown in Fig. 11, the boundary of the gripping arm to which the microsphere adheres is connected with that of the plunger. Thus, only two contours are detected with the larger contour containing the microsphere. By comparing the y-coordinates of the centroids of the contours (see M_1 and M_2 in Fig. 11), the system determines to which gripping arm the microsphere adheres.

B. Contact Detection and Microrobotic Control

Knowledge of relative depth positions of the gripping arms and microsphere is gained through the detection of the contact between the gripping arms and the surface of the substrate. Obviating the need for additional force/touch sensors, the system employs a vision-based contact-detection algorithm [36] that provides a detection accuracy of 0.2 μm. The contact-detection process completes within 5–8 s.
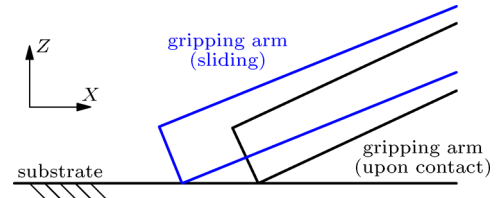
Fig. 12.   Vision-based contact detection. Gripping arms slide on the substrate after contact is established.
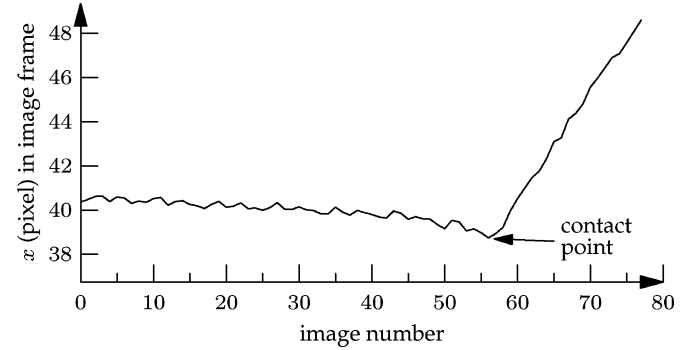
Fig. 13.   Contact detection by monitoring x-coordinate of a gripping arm in the image while lowering the microgripper at a speed of 20 μm/s.

The microgripper was controlled to move downward at a constant speed (e.g., 20 μm/s) to establish a contact with the substrate while the algorithm ran in real time. Since further lowering the gripping arms after the contact is established causes the gripping arms to slide on the substrate (see Fig. 12), monitoring the x-coordinates of the gripping arms result in a V-shaped curve, as shown in Fig. 13. The global minimum represents the initial contact of the microgripper with the substrate.

The microrobotic system is a "looking-and-moving" system. Transformation between the image frame (x–y) and the microrobot frame (X–Y) was achieved with calibrated pixel sizes. With the centroid and radius of a target microsphere recognized, the microrobot moves the microgripper to the target position via a proportional–integral–differential (PID) controller.

C. Automated Pick-and-Place of Microspheres

To quantify the operation speed of the microrobotic system, microspheres were picked and placed to form patterns. The system starts with the contact detection to determine the depth position of the gripping arms relative to the substrate surface. The microgripper was then moved upward by 15 μm above the substrate, which was ready for the pick-and-place operation.

Microspheres in the field-of-view were visually recognized. Their positions in the image frame, sizes, and optimal grasping positions were determined. Then, by using the contact-detection result and coordinate transformation, the target X–Y–Z positions were determined by the system. The microspheres were picked up from the source area in the order of their x-coordinates in the image frame. According to the actuation calibration results (see Fig. 3), the system determined actuation voltages for the gripping arms for secured grasping while ensuring that no excessively large actuation voltages were applied.

The microrobot lifted the securely grasped microsphere to 15 μm above the substrate. When a preplanned target position was reached, the microrobot moved downward and stopped at 2 μm above the substrate for release. The gripping arm to which the microsphere adhered was
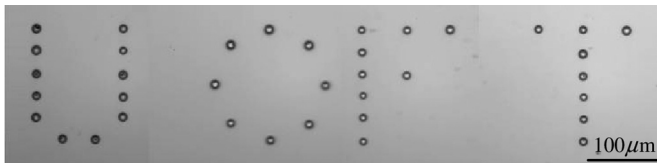
Fig. 14.   Pattern formation by automated pick-and-place. (a) Microspheres before pick-and-place. (b) Circular pattern with circularity of 0.52 μm.
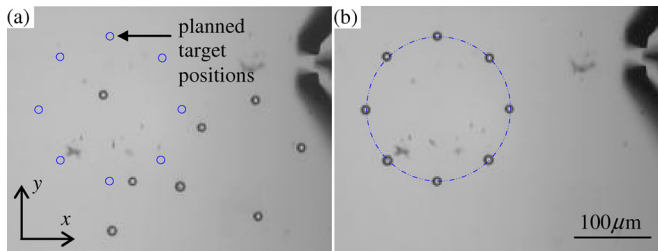
Fig. 15.   "U of T" pattern formed by automated microrobotic pick-and-place of 7.5–10.9 μm microspheres.
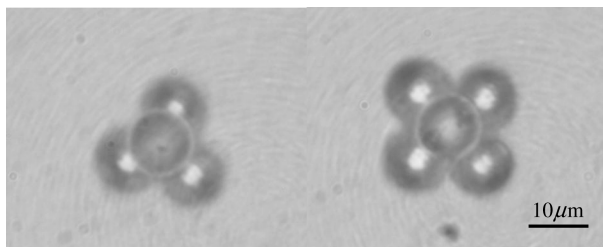
Fig. 16.   Microspheres assembled into two-layered structures.

first visually detected and then aligned the microsphere accurately in front of the plunger based on the calibration results, as shown in Fig. 3. The plunger was then actuated to release the microsphere, after which, the microgripper was raised 15 μm above the substrate and returned to the source area to pick up the next microsphere. Fig. 14 shows that microspheres were arranged into a circular pattern with a circularity of 0.52 μm, which is defined as the standard deviation of the distances from the microspheres to the center of the circle. Fig. 15 shows an assembled "U of T" (University of Toronto) pattern. The average pick-and-place speed was 6 s/sphere.

D. Three-Dimensional Assembly of Microspheres

The technique can be extended to building 3-D structures (e.g., see Fig. 16). The difficulty involved in such tasks is that the microgripper tips, when positioning a microsphere for release, may collide with other microspheres in close proximity. To overcome this difficulty, a rotational DOF is required in the system, either for the substrate and thus, the microspheres, or for the microgripper to avoid collision between the microgripper tips and microspheres.

VI. CONCLUSION

The microrobotic system presented in this paper is capable of high-speed, fully automated pick-and-place operation of microobjects. The paper reported an effective pick-and-place technique employing a new MEMS microgripper that integrates both gripping and release mechanisms. The microgripper was applied to the grasping and active release

of 7.5–10.9 μm microspheres. The plunger provides the microsphere with sufficient momentum to overcome adhesion forces, thus resulting in highly repeatable release (100% of 700 trials) and a release accuracy of 0.45$\pm$0.24 μm. Enabled by this releasing technique, an automated robotic pick-and-place system was realized using vision-based techniques for the recognition of the microgripper and microspheres, determination of the height of the microgripper above the substrate, and motion control of the microrobot. The system demonstrated a pick-and-place speed of 6 s/sphere, which is much faster than a skilled operator and an order of magnitude faster than the highest speed reported in the literature thus far. Three-dimensional structures were also built with microspheres to demonstrate the capability of 3-D assembly.

There are limitations in the size, geometry, and material of microobjects that can be manipulated by the microrobotic system. In consideration of the structural dimensions of the present device (e.g., thickness of the gripping arms and plunger of 25 μm and initial gripping-arm opening of 17 μm), the size of microobjects suitable for manipulation can be up to 17 μm. With regard to the geometry, it is speculated that this technique is effective to manipulate symmetrical objects, such as microcubes and triangular objects, if the shape of the microgripper tips is modified to conform to the object. For irregular-shaped microobjects, however, this technique might not be effective because the orientation control of microobjects and the plunger alignment can be difficult. As for materials with a higher surface energy than glass, it is believed that the object can still be successfully released as long as it gains sufficient momentum from the plunging impact.

REFERENCES

[1] C. D. Onal and M. Sitti, "Visual servoing-based autonomous 2-D manipulation of microparticles using a nanoprobe," *IEEE Trans. Control Syst. Technol.*, vol. 15, no. 5, pp. 842–852, Sep. 2007.
[2] K. F. Böhringer, R. S. Fearing, and K. Y. Goldberg, "Microassembly," in *Handbook of Industrial Robotics*, S. Y. Nof, Ed. New York: Wiley, 1999, pp. 1045–1066.
[3] S. Fatikow, J. Seyfried, S. Fahlbusch, A. Buerkle, and F. Schmoeckel, "A flexible microrobot-based microassembly station," *J. Intell. Robot. Syst.*, vol. 27, pp. 135–169, 2000.
[4] J. A. Thompson and R. S. Fearing, "Automating microassembly with ortho-tweezers and force sensing," in *Proc. IEEE/RSJ Int. Conf. Intell. Robot. Syst.*, Maui, HI, Oct. 2001, pp. 1327–1334.
[5] G. Yang, J. A. Gaines, and B. J. Nelson, "A supervisory wafer-level 3D microassembly system for hybrid MEMS fabrication," *J. Intell. Robot. Syst.*, vol. 37, pp. 43–68, 2003.
[6] N. Dechev, W. L. Cleghorn, and J. K. Mills, "Microassembly of 3-D microstructures using a compliant, passive microgripper," *J. Microelectromech. Syst.*, vol. 13, no. 2, pp. 176–189, 2004.
[7] A. Ferreira, C. Cassier, and S. Hirai, "Automatic microassembly system assisted by vision servoing and virtual reality," *IEEE/ASME Trans. Mechatron.*, vol. 9, no. 2, pp. 321–333, Jun. 2004.
[8] K. Tsui, A. A. Geisberger, M. Ellis, and G. D. Skidmore, "Micromachined end-effector and techniques for directed MEMS assembly," *J. Micromech. Microeng.*, vol. 14, pp. 542–549, 2004.
[9] A. M. Hoover and R. S. Fearing, "Rapidly prototyped orthotweezers for automated microassembly," in *Proc. IEEE Int. Conf. Robot. Autom.*, Rome, Italy, Apr. 2007, pp. 812–819.
[10] D. Hériban and M. Gauthier, "Robotic micro-assembly of microparts using a piezogripper," in *Proc. IEEE/RSJ Int. Conf. Intell. Robot. Syst.*, Nice, France, Sep. 2008, pp. 4042–4047.
[11] M. Mayyas, P. Zhang, W. H. Lee, D. Popa, and J. C. Chiao, "An active micro joining mechanism for 3D assembly," *J. Micromech. Microeng.*, vol. 19, pp. 035012-1–035012-12, 2009.
[12] R. S. Fearing, "Survey of sticking effects for micro-parts," in *Proc. IEEE/RSJ Int. Conf. Intell. Robot. Syst.*, Pittsburgh, PA, Aug. 1995, pp. 212–217.
[13] F. García-Santamaría, H. T. Miyazaki, A. Urquía, M. Ibisate, M. Belmonte, N. Shinya, F. Meseguer, and C. López, "Nanorobotic manipulation of microspheres for on-chip diamond architectures," *Adv. Mater.*, vol. 16, pp. 1144–1147, 2002.

[14] K. Aoki, H. T. Miyazaki, H. Hirayama, K. Inoshita, T. Baba, K. Sakoda, N. Shinya, and Y. Aoyagi, "Microassembly of semiconductor three-dimensional photonic crystals," *Nat. Mater.*, vol. 2, pp. 117–121, 2003.

[15] A. Tafazzoli, C.-M. Cheng, C. Pawashe, E. K. Sabo, L. Trofin, M. Sitti, and P. R. LeDuc, "Subfeature patterning of organic and inorganic materials using robotic assembly," *J. Mater. Res.*, vol. 22, pp. 1601–1608, 2007.

[16] S. Saito, H. T. Miyazaki, T. Sato, and K. Takahashi, "Kinematics of mechanical and adhesional micromanipulation under a scanning electron microscope," *J. Appl. Phys.*, vol. 92, pp. 5140–5149, 2002.

[17] O. Fuchiwaki, A. Ito, D. Misaki, and H. Aoyama, "Multi-axial micromanipulation organized by versatile micro robots and micro tweezers," in *Proc. IEEE Int. Conf. Robot. Autom.*, Pasadena, CA, May 2008, pp. 893–898.

[18] W. Driesen, T. Varidel, S. Régnier, and J.-M. Breguet, "Micro manipulation by adhesion with two collaborating mobile micro robots," *J. Micromech. Microeng.*, vol. 15, pp. S259–S267, 2005.

[19] S. Saito and M. Sonoda, "Non-impact deposition for electrostatic micromanipulation of a conductive particle by a single probe," *J. Micromech. Microeng.*, vol. 18, pp. 107001-1–107001-3, 2008.

[20] D. S. Haliyo, S. Régnier, and J.-C. Guinot, "[mü]mad, the adhesion based dynamic micro-manipulator," *Eur. J. Mech. A*, vol. 22, pp. 903–916, 2003.

[21] Y. Fang and X. Tan, "A dynamic JKR model with application to vibration release in micromanipulation," in *Proc. IEEE/RSJ Int. Conf. Intell. Robot. Syst.*, Beijing, China, Oct. 2006, pp. 1341–1345.

[22] W. Zesch, M. Brunner, and A. Weber, "Vacuum tool for handling microobjects with a nanorobot," in *Proc. IEEE Int. Conf. Robot. Autom.*, Albuquerque, NM, Apr. 1997, pp. 1761–1766.

[23] B. López-Walle, M. Gauthier, and N. Chaillet, "Principle of a submerged freeze gripper for microassembly," *IEEE Trans. Robot.*, vol. 24, no. 4, pp. 897–902, Aug. 2008.

[24] F. Arai, D. Andou, Y. Nonoda, T. Fukuda, H. Iwata, and K. Itoigawa, "Integrated microendeffector for micromanipulation," *IEEE/ASME Trans. Mechatron.*, vol. 3, no. 1, pp. 17–23, Mar. 1998.

[25] D. H. Kim, M. G. Lee, B. Kim, and Y. Sun, "A superelastic alloy microgripper with embedded electromagnetic actuators and piezoelectric force sensors: a numerical and experimental study," *Smart Mater. Struct.*, vol. 14, pp. 1265–1272, 2005.

[26] N. Chronis and L. P. Lee, "Electrothermally activated SU-8 microgripper for single cell manipulation in solution," *J. Microelectromech. Syst.*, vol. 14, pp. 857–863, 2005.

[27] F. Beyeler, A. Neild, S. Oberti, D. J. Bell, Y. Sun, J. Dual, and B. J. Nelson, "Monolithically fabricated microgripper with integrated force sensor for manipulating microobjects and biological cells aligned in an ultrasonic field," *J. Microelectromech. Syst.*, vol. 16, pp. 7–15, 2007.

[28] K. Kim, X. Liu, Y. Zhang, and Y. Sun, "Nanonewton force-controlled manipulation of biological cells using a monolithic MEMS microgripper with two-axis force feedback," *J. Micromech. Microeng.*, vol. 18, pp. 055013-1–055013-8, 2008.

[29] O. Sardan, V. Eichhorn, D. H. Petersen, S. Fatikow, O. Sigmund, and P. Bøggild, "Rapid prototyping of nanotube-based devices using topology-optimized microgrippers," *Nanotechnol.*, vol. 19, pp. 495503-1–495503-9, 2008.

[30] B. K. Chen, Y. Zhang, and Y. Sun, "Active release of microobjects using a MEMS microgripper to overcome adhesion forces," *J. Microelectromech. Syst.*, vol. 18, pp. 652–659, 2009.

[31] F. Arai, D. Ando, and T. Fukuda, "Adhesion forces reduction for micro manipulation based on microphysics," in *Proc. Int. Workshop Micro Electro Mech. Syst.*, San Diego, CA, Feb. 1996, pp. 354–359.

[32] Y. Zhou and B. J. Nelson, "Adhesion force modeling and measurement for micromanipulation," in *Proc. SPIE Conf. Microrobot. Micromanipulation*, Boston, MA, Nov. 1998, pp. 169–180.

[33] R. A. Bowling, "A theoretical review of particle adhesion," in *Particles on Surfaces I: Detection, Adhesion and Removal*, K. L. Mittal, Ed. New York: Plenum, 1988, pp. 129–155.

[34] J. N. Israelachvili, *Intermolecular and Surface Forces*, 2nd ed. New York: Academic, 1992.

[35] W. Ding, H. Zhang, and C. Cetinkaya, "Rolling resistance moment-based adhesion characterization of microspheres," *J. Adhes.*, vol. 84, no. 12, pp. 996–1006, 2008.

[36] W. H. Wang, X. Y. Liu, and Y. Sun, "Contact detection in microrobotic manipulation," *Int. J. Robot. Res.*, vol. 26, pp. 821–828, 2007.